(PHOTO)ELECTROCHEMISTRY: A SUITABLE TOOL FOR INVESTIGATING WET ETCHING PROCESSES ON III-V SEMICONDUCTORS

H. H. GOOSSENS* and W. P. GOMES

Rijksuniversiteit Gent, Laboratorium voor Fysische Scheikunde, Krijgslaan 281, B-9000 Gent, Belgium

(Received 1 July 1991)

Abstract—Wet etching processes at III-V semiconductors are studied both from the viewpoint of the reaction mechanisms and from that of the morphology of the etched surfaces. Emphasis is put on GaP single crystals, for which four different types of etching are considered, ie (photo)anodic, electroless, chemical and photoetching. Relations between etching kinetics, crystallographic orientation and etching morphology are discussed. These relations, as well as observed differences in etch morphology between n- and p-type crystals, are shown to be very often interpretable on the basis of electrochemical concepts as established by (photo)anodic studies.

Key words: semiconductor, photoelectrochemistry, etching mechanism, electrode kinetics, surface morphology.

1. INTRODUCTION

Today's electronics industry is witnessing an increasing interest in III-V compound semiconductors as electronic and optoelectronic materials. Etching, the controlled dissolution of semiconductors, has become an essential process in microelectronic device technology[1, 2]. Indeed, most devices consist of multilayer systems, the fabrication of which can be essentially described as the subsequent epitaxial stacking of thin layers and the selective removal of small parts of these layers according to well-defined patterns. This selective removal can be performed either by masking the semiconductor surface[3, 4] or, in the case of lightsensitive etching, by local illumination using a laser beam[5, 6]. Specific applications of etching procedures in the production of electronic devices are, eg the fabrication of diffraction gratings for solid-state lasers by holographic photoelectrochemical etching[7] and the photoelectrochemical etching of integral lenses on LEDs for efficient coupling to optical fibers[8]. Etching procedures are furthermore used to reveal different kinds of crystal defects such as dislocations. impurity striations and microprecipitates[9-11] and hence constitute a fast and easy way for quality control. Crystallographers often use etching procedures for the identification of crystal planes, owing to the fact that the surface morphology after etching often depends on the crystal orientation[12-14]. Finally, etching procedures are widely used to remove various kinds of unwanted surface layers (such as oxide layers or damaged layers), which are present as a consequence of different pretreatment processes, in order to obtain a clean and well-defined surface[15]. It is hence important, not only from the fundamental but

Etching can be performed by using either "wet" or "dry" procedures [15-17]. In the case of dry etching, the active species are charged or neutral gaseous particles (ions and radicals). This type of etching may proceed either by chemical interaction between the semiconductor surface and the reactive species (being in most cases free radicals), in which case the reaction products volatilize, or by bombardment of the surface by ions leading to the sputtering of surface atoms or, as is usually the case, by a combination of both effects. In wet etching processes, the removal of material originates from a chemical and/or electrochemical reaction at the semiconductor/electrolyte interface. It is the aim of this article to show that (photo)electrochemical methods may be quite successful in the study of wet etching processes on III-V semiconductors, not only in order to unravel the reaction mechanisms, but also to get a deeper insight into the origin of the surface morphology after etching. Relying upon (photo)electrochemical concepts, answers will be sought to intriguing questions such as why in the case of GaP in alkaline medium, etching by Fe(CN)₆³ in darkness usually leads to morphologies which are different for the (111)- and the (III)face, independent of the semiconductor type, whereas etching by OBr under illumination leads to etch patterns which are similar for both polar faces but completely different for n- and p-type samples.

Wet etching processes may proceed either under conditions in which the sample is simply immersed into the etchant solution or under external current flow. In the latter case, the semiconductor crystal is incorporated as an electrode in an electrochemical cell and polarized anodically under illumination or in darkness for n- and p-type samples, respectively,

also from the technological point of view, to get a deeper insight into the factors governing the rates and the morphology and hence into the mechanisms of etching of semiconductors.

^{*}Research Assistant of the N.F.W.O. (National Fund for Scientific Research, Belgium).

leading to the dissolution of the sample. The anodic dissolution reactions of III-V semiconductors have constituted a subject of great interest during the last decade, the more so since these decomposition reactions constitute a major problem when using n-type semiconductor electrodes in photoelectrochemical solar cells. As far back as the 1960s, Gerischer[18, 19] showed in the case of GaAs that the oxidation reaction requires six electronic charge carriers (mainly holes) for each GaAs surface entity dissolved, and that chemical reactions involving either H₂O molecules or OH- ions play an important role in the dissolution process. Memming and Schwandt[20] demonstrated that in alkaline solutions OH- ions are consumed in the electrochemical dissolution of GaP. The detailed mechanisms of the anodic decomposition of III-V semiconductors such as GaAs, GaP and to a lesser extent InP, have been extensively studied by several authors[21-28]. These studies will not be treated in detail here; emphasis will primarily be put on the morphology of the photoanodically etched surfaces. the interpretation of which will be based upon the dissolution kinetics. As a starting point, the discussion will make use of our recent study on the interrelation between kinetics and morphology in the (photo)anodic dissolution of [111]- and [100]-oriented GaP single crystals in alkaline (partly published in Ref. [29]) as well as in acidic aqueous solutions. As will be demonstrated in the case of GaP, such a study also constitutes a basis for understanding the mechanisms and the resulting morphology of etching processes which do not involve external current flow, denoted in what follows as open-circuit etching processes.

Gerischer[18, 19, 30-32] was probably the first to recognize the potential of semiconductor electrochemistry for investigating the mechanisms of open-circuit etching processes. He showed that for dark opencircuit etching, two different types of mechanism may operate. The first type is an electrochemical mechanism, in which the anodic oxidation of the semiconductor by holes is electrically compensated by the cathodic reduction of a dissolved oxidizing agent via the valence band, ie through injection of holes. This type of etching process, called "electroless" etching, holds, for example, in the case of GaAs etching in alkaline K₃Fe(CN)₆ solutions[18] and in acidic Ce4+ solutions[19] and is characterized by the fact that it is influenced by polarization of the semiconductor: when the sample is polarized cathodically, the injected holes migrate into the interior of the semiconductor crystal, so that they are no longer available at the surface to etch the semiconductor. The alternative type of process is purely "chemical" etching[19, 30-32] in which no holes are injected by the etching reactant and hence no free electronic charge carriers are involved. Etching in this case may also proceed under cathodic polarization of the semiconductor crystal, although at n-type crystals it is often found that the chemical attack by the oxidizing agent is suppressed by the cathodic reduction of this reactant via the conduction band, ie when the latter reaction is diffusion-limited. A chemical etching mechanism was shown to hold for the etching of GaAs by symmetrical bifunctional oxidizing agents such as Br2, I_2 and $H_2O_2[19, 30-32]$. Gerischer[19] proposed a concerted mechanism for this type of reaction, in which bonds are broken between reactant atoms and between surface atoms and new bonds are formed between surface and reactant atoms almost simultaneously.

Also for dark open-circuit electroless and chemical etching processes, the present discussion will be focused upon GaP single crystals. It will be shown that even in the case of chemical etching, an electrochemical study of the interface may yield valuable information on the mechanism, which in certain cases appears to be different from that proposed by Gerischer. Emphasis will also be put upon the morphology of the etched surfaces and a comparison will be made between the morphology after anodic, electroless and chemical etching.

From the technological point of view, photoetching, ie wet open-circuit etching under illumination, is a most attractive procedure. Indeed, it does not require any electrical contacts and it reveals crystallographic imperfections with a very high resolution and sensitivity[33-37]. Furthermore, it can be applied locally by using focussed light, eg laser light, which makes the method attractive for maskless micromachining purposes[38-40]. The mechanisms of photoetching processes are electrochemical, both under uniform or under non-uniform illumination of the semiconductor surface[41, 42]. Electron-hole pairs are created by illumination; the conduction band electrons reduce an oxidizing agent present in solution, whereas the holes oxidize the semiconductor. Thus, as in the case of electroless etching in darkness, two partial currents flow through the interface, which cancel each other electrically but not chemically. In the case of nonuniform illumination of the semiconductor surface, these two partial currents are macroscopically separated in space. At an n-type semiconductor, the illuminated area plays the role of a local anode, at which the semiconductor is dissolved, whereas the non-illuminated area acts as a local cathode, at which reduction of the oxidizing agent takes place; the opposite holds for p-type samples[33, 43]. Hence on the whole, the sample behaves as a corroding galvanic cell[42]. The role of electrochemistry in the investigation of (photo)etching processes will be illustrated again mainly on the basis of GaP, for which the link between (photo)anodic and photoetching processes will be shown. Again, the importance of electrochemical principles for the interpretation of the surface morphology will be demonstrated.

It is hence the aim of this paper to show that a photoelectrochemical study of the semiconductor/ electrolyte interface leads to a deeper and more fundamental insight into wet etching processes, not only as far as the etching mechanism but also the surface morphology is concerned. Especially in view of the latter objective, it will appear to be essential to compare the results of studies on all four types of etching processes mentioned.

2. EXPERIMENTAL

The GaP single crystals were purchased from MCP Electronics (UK). The n-type samples were sulphurdoped, whereas the p-type samples were zinc-doped. The donor density was 6.2×10^{17} – 9.6×10^{17} cm⁻³

and 4.0×10^{17} cm⁻³ for n-type crystals oriented along the [111]- and [100]-axis, respectively. The acceptor density in the p-type samples amounted to 10¹⁸ cm⁻³ and 1.4×10^{17} – 8.0×10^{17} cm⁻³, respectively, for the orientations mentioned. Ohmic contacts were made by evaporating In or an In + Zn (5%) alloy in vacuo on n- and p-type respectively, and by subsequently heating at 400°C in N2. After fixing the crystal onto a copper rod by means of a conductive silver paste and mounting it in a PVC holder by using an insulating epoxy resin, the specimen was ground on abrasive paper and subsequently polished on Al₂O₃-powder (final polish 0.05 μ m). Then, the crystal was (photo)anodically etched in a KOH solution (pH = 13) at a diffusion-limited rate in order to remove mechanicallyinduced surface damage[29].

Etch rates were measured by using a so-called flow cell, ie a microelectrochemical cell with continuous electrolyte flow and in which the electrolyte was collected at the exit and subsequently analysed for dissolved Ga(III). More details on the flow cell and on the spectrophotometric analysis of Ga(III) are given in Refs [29, 44-46]. The kinetics of the electrochemical reactions taking place at the semiconductor/electrolyte interface were studied by means of rotating disk and ring-disk voltammetry, the experimental set-up of which is also described in more detail in the aforementioned references.

The morphology of the surface after etching was studied by using a microscope-interferometer[29] and a Talystep apparatus.

3. RESULTS AND DISCUSSION

3.1. (Photo)anodic etching

3.1.1. (Photo)anodic etching of GaP in alkaline solutions. As already mentioned, (photo)anodic polarization of GaP leads, as for most III-V semiconductors, to oxidation and hence, at either low or high

pH, to dissolution (etching) of the semiconductor. By comparing the anodic current density to the corresponding etch rate, as determined by the flow cell technique, the anodic dissolution in alkaline solutions was found to consume six elementary charge carriers per formula unit of GaP. This result, which was obtained at all three crystal surfaces investigated and which was independent of the anodic potential, the current density, the light intensity and the flow rate of the electrolyte, is in contrast with the early results of Memming and Schwandt[20] but confirms the later reports of Meek and Schumaker[47] and Madou et al. [48]. At pH = 13, the anodic oxidation reaction of GaP can hence be written as[49]

$$GaP + 6h^{+} + 11OH^{-}$$

 $\rightarrow GaO_{3}^{3-} + HPO_{3}^{2-} + 5H_{2}O_{3}$ (1)

if one considers all electronic charge carriers involved to be holes (in fact, a small fraction of the charge transfer has been shown to occur via the conduction band, *ie* by injection of electrons[48, 50]).

Studying the voltammetric behaviour of p-GaP in KOH solutions of pH = 13, it was found that at high anodic polarization, V, the current density i reaches a plateau, limited by the rate of OH- ion diffusion towards the semiconductor surface. A current densitypotential curve, registered at a (100) p-GaP electrode is shown in Fig. 1; the insert represents the variation of the limiting anodic current density with the square root of the rotation rate w (Levich behaviour). The limiting current density was furthermore found to be proportional to the OH- concentration at pH values between 11 and 13. Analogous results were obtained at the (III)- and (111)-faces[44]. The exponentially rising part of the i-V curve depended somewhat on the crystal face, the Tafel slope amounting to 100-110 mV at the (100)-face, to 90-100 mV at the (III)-face and to 140-150 mV at the (111)-face[29].

The photoanodic current density-potential curve of n-GaP also shows a plateau region which, in KOH

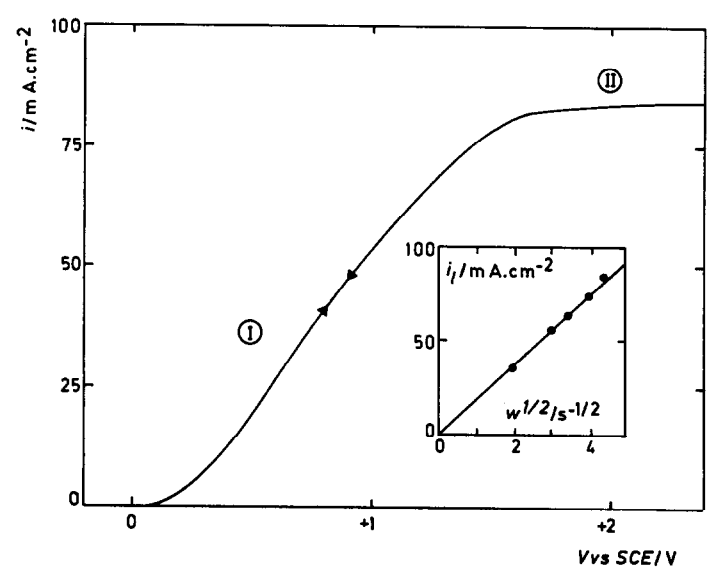


Fig. 1. Current density-potential curve at a dark (100) p-GaP rotating electrode in aqueous KOH (pH = 13). Rotation rate $w = 20 \text{ s}^{-1}$; scan rate = 10 mV s⁻¹. Insert: limiting current density i_1 as a function of $w^{1/2}$, V = +2.2 V vs. sce.

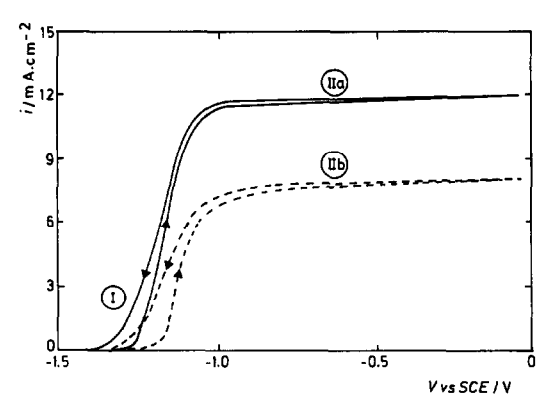


Fig. 2. Current density-potential curve at an illuminated (100) n-GaP flow-cell electrode in aqueous KOH (pH = 13). Flow rate = 50 ml h⁻¹; scan rate = 1 mV s⁻¹. (——) Full light intensity; (---) 24% of full light intensity.

(pH = 13) solutions, was found to be independent of the rotation rate of the electrode and proportional to the light intensity at relatively low light intensities, but to be rotation-rate dependent and independent of the light intensity at high values of the latter[44]. Figure 2 shows as an example the photoanodic current density curves registered at (100) n-GaP under full light intensity, in which case the limiting value is controlled by the OH⁻ diffusion rate, and at 24% of full light intensity, in which case the limiting value is controlled by the light intensity. The onset region of these curves is mainly controlled by surface charge-carrier recombination.

The interpretation of the observed voltammetric behaviour is straightforward. Considering reaction equation (1) describing the anodic dissolution of GaP, it is obvious that the detailed reaction mechanism must involve electrochemical steps in which decomposition intermediates of increasing oxidation state are formed, as well as chemical steps in which OH^- ions react with the decomposition intermediates. In the steady state, the rates of all subsequent electrochemical steps must be equal, so that the rate can be expressed as that of the first step, in which a GaP surface bond captures a hole, leading to the formation of a first intermediate X_1^+ with one electron-deficient bond:

$$X_0 + h^+ \xrightarrow{k} X_1^+. \tag{2}$$

In equation (2), X_0 stands for a non-oxidized GaP surface entity.

At low photoanodic current densities (and hence low etch rates), the rate-determining step can be assumed to be electrochemical. This explains the exponential dependence of the anodic current density on the potential at p-GaP (Fig. 1, region I) and the light-intensity dependence of the photocurrent density at n-GaP at low light intensities (Fig. 2, region IIb). Although Tafel slopes above 60 mV are not fully understood[51], the difference in Tafel slope between the two polar (111)-faces can be interpreted as a difference in reactivity of X_0 towards holes, which in turn may be attributed to the different orientation of the Ga-P dipole at both faces[29]: at the (III)-face, the dipole field is oriented in such a way that is energetically favourable for the holes to reach the

surface, whereas at the (111)-face, it is oriented in the opposite way. The reactivity of the (100)-face, which is very similar to that of the (III)-face (similar Tafel slopes), will be discussed further.

At high (photo)anodic current densities, the ratedetermining step will no longer be an electrochemical one, but a chemical reaction between an OH⁻ ion and a decomposition intermediate, the rate of which is limited by diffusion of OH⁻ ions towards the GaP surface. This explains the photoanodic current plateau at p- and n-GaP at high light intensities.

In view of the study of the correlation between etching kinetics and etching morphology, the following kinetic regions should be considered. For p-GaP, distinction has to be made between the exponential region I (Fig. 1) of the i-V curve, in which the current density is determined by the hole capture rate, and the plateau region II (Fig. 1), in which the anodic current and hence the etch rate is determined by diffusion of OH⁻ ions towards the surface. For n-GaP, distinction has to be made between the photocurrent onset region I (Fig. 2), in which surface recombination of the charge carriers predominates, and the photocurrent plateau region II, in which the plateau current is controlled either by OH- diffusion (region IIa, high light intensities) or by the light-intensity dependent creation of electron-hole pairs (region IIb. low light intensities).

Experimentally if was found, for all three crystal faces studied, that etching at a diffusion-limited rate (region II, Fig. 1; region IIa, Fig. 2) leads to a flat surface. This is simply explained by the fact that for a diffusion-limited process, the etch rate is the same over the whole surface and is hence unaffected by solid-state factors.

When etching at a rate below the diffusion limit, specific etch patterns develop at the surface, due to local differences in the rate of the surface reaction. When etching p-GaP in the rising part of the i-V curve (Fig. 1, region I), etch pits develop at the surface with a density of 10^5-10^6 cm⁻² and with a geometry depending on the crystal orientation (Fig. 3): the pits at the (III)- and (111)-faces exhibit a more or less equilateral-triangular shape, whereas those at the (100)-face are roughly rectangular. Furthermore, it is important to note that at the (111)-face, etch pits with a depth of the order of 1 μ m and a width of the order of 10 μ m are visible after removal of a layer of 10 μ m or less in thickness only, whereas at the (III)- and (100)-faces, several tens of μ m have to be removed before the etch pits can be distinguished. This difference in selectivity can be explained as follows. In the case of a p-type semiconductor, holes constitute the majority carriers and are hence spread out at the surface in a quasi-equilibrium cloud[29, 52]. Surface bonds at dislocations and impurity sites may be assumed to be weaker than those at intact sites[29], resulting in an enhanced hole capture rate and hence in the formation of etch pits at these sites. Assuming the reactivity at these defect sites to be unaffected or hardly affected by the crystal orientation, the observed difference in selectivity between the (111)- and (III)faces can be attributed to the above cited difference in the hole capture reactivity between the (111)- and the (III)-faces at intact sites, which is due to the difference in the Ga-P surface dipole orientation

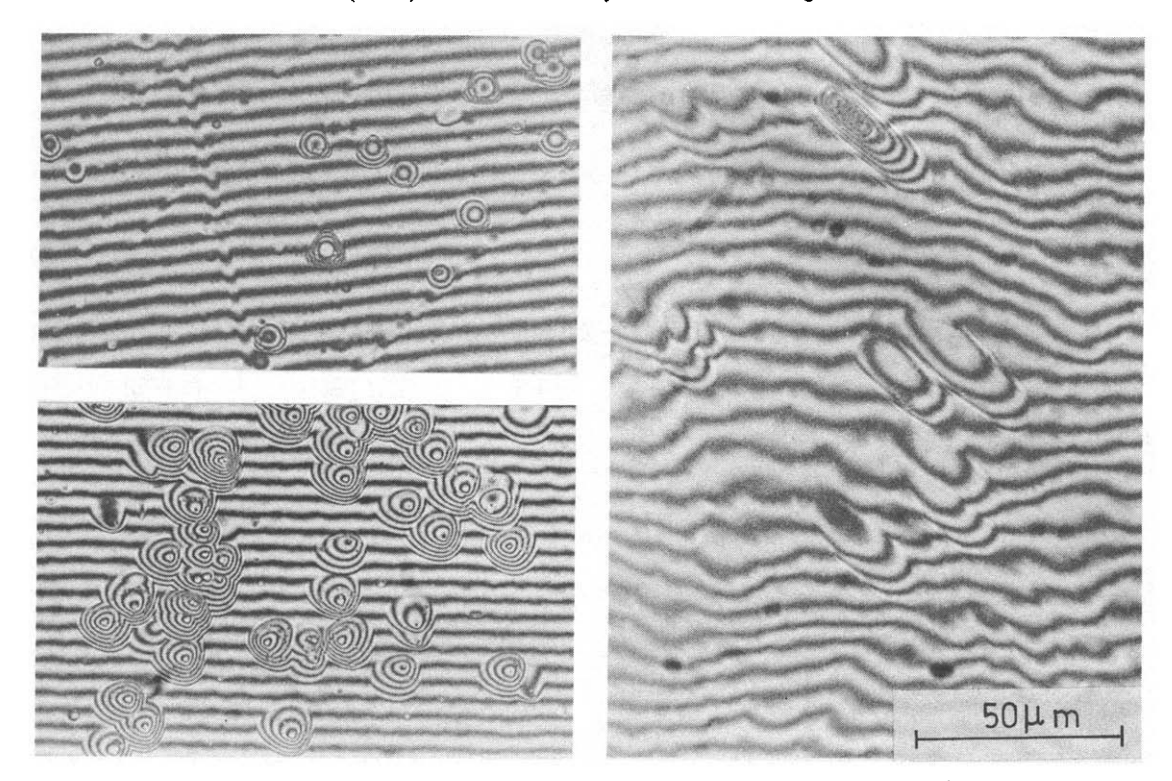


Fig. 3. Interference photomicrograph of a p-GaP surface after etching at i = 4.5 mA cm⁻² in aqueous KOH (pH = 13). Left: top, (III)-face, etching time = 6 h; bottom, (111)-face, etching time = 0.5 h. Right: (100)-face, etching time = 18 h.

(polarity along the [111]-axis). The similarity in selectivity of the (III)- and the (100)-faces must then be attributed to a similarity in hole capture reactivity at undisturbed (III)- and (100)-surface sites, experimental evidence for which is found in the comparable values of the Tafel slopes. Note that in general, the (III)- and (100)-faces of III-V semiconductors are etched at comparable rates but considerably faster than the (111)-face [13, 15, 40, 53-63]. In order to explain this, let us first consider the shape of the etch pits developed at the different faces, which reflects the symmetry of the crystal lattice along the axis concerned (the [111] trigonal axis and the [100] tetragonal inversion axis, hence exhibiting digonal symmetry). The formation of rectangularly shaped etch pits at the (100)-face of III-V semiconductors has been suggested to result from the polarity of the lattice along the [111]-direction[13, 55]. It has been assumed that one pair of opposite sides of the pit consists of group III atom {111} planes, whereas the other pair of opposite sides consists of group V atom {111} planes. The rectangular shape then would arise from the fact that the group V atom {111} planes etch faster than the group III atom {111} planes, so that the longer sides of the pit would correspond to the group III atom {111} planes and the shorter sides to the group V atom {111} planes. This explanation however is not consistent with the observation that etch grooves, obtained by profile etching of (100)-faces[13, 54, 64], contain group III atom {111} planes in both perpendicular directions, leading to a V-shaped and a reverse mesa-shaped ("dovetail") profile of an etched groove in the [011]- and [011]-direction respectively

(see Fig. 4). We will therefore assume here that the same planes are formed when the etching proceeds at a defect site of an unmasked surface (it is indeed a generally accepted idea that recessed etch figures are bound by planes of low etch rates, the intersections corresponding to high etch rates[12]). As the Ga

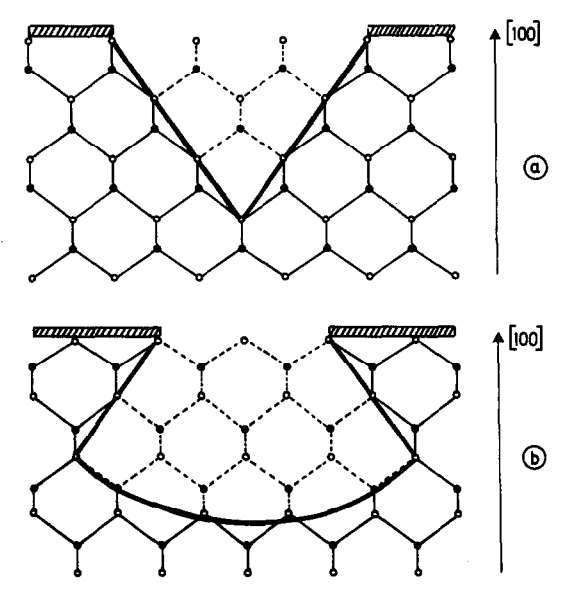


Fig. 4. Schematic representation of the cross section of a groove obtained by profile etching of the (100)-face. (a) Mask opening aligned in the [011]-direction; (b) mask opening aligned in the [011]-direction.

{111}-faces developed converge in one direction, whereas they diverge in the perpendicular direction (cf. Fig. 4), the top view of an etched pit at the (100)-face appears as a rectangle. The assumption that Ga {111}-faces with the orientations mentioned are developed implies that the etching proceeds in directions perpendicular to the {111}-faces in pairs of {111}-faces and that these pairs are etched faster from the P-side than from the Ga-side. Experimental evidence for the idea that the etching of {111}-faces proceeds by pairs, with the P-side etched faster than the Ga-side, follows from the different etching behaviour of the (III)- and (111)-faces. The assumption that the etching of the (100)-face actually proceeds perpendicularly to the {111}-faces may explain the similar etch reactivity of the (100)- and (111)-faces, since for the (100)-face, the opportunity always exists to etch the {111}-face pairs from the P-side.

When etching n-GaP photoanodically in the onsetregion I of the photocurrent-potential curve (Fig. 2), etch hillocks and ridges are observed at the surface after removal of only a small amount of material (in Fig. 5 eg hillocks of about $0.5 \mu m$ high are visible after removal of a layer which we calculated from analytical results to be about $0.5 \mu m$ thick, indicating that at the sites of the elevated structures essentially no etching takes place). The formation of these structures is explained by considering that in the onset-region, recombination of charge carriers predominates. Dislocations and damaged sites lead to localized energy states which may act as efficient recombination centers[65], hence resulting in a lower local surface concentration of holes. The fact that these sites are developed as hillocks (ie are being etched at a lower rate than their surroundings) indicates that the enhanced reactivity at the defect sites

is overcompensated by the reduced concentration of holes. This may also explain the observation that no distinction is seen between the (100)-, (III)- and (111)-faces.

In the photocurrent plateau region IIb, in which the photocurrent density is determined by the light intensity, etching of n-GaP (III) and (100) crystal faces leads to a microrough surface, with a few scratches developed as elevated chains, whereas at the (111)-face isosceles triangular pits are formed with three orientations making 120° angles, often forming starlike configurations (Fig. 6). The morphology of the (III)- and (111)-face was already discussed in detail in a previous paper[29]. It was proposed that, in contrast to p-GaP, the holes at the n-GaP surface do not constitute a quasi-equilibrium cloud, since they are created in the semiconductor by light and move through the space-charge region to the surface, where they react almost immediately. The microroughness of the (III)-face is interpreted by assuming that the flow of the holes through the space-charge layer is non-homogeneous, due to the presence of the donors, a concept which has been introduced by Tenne et al. [66-68] in their work on II-VI semiconductors. The few ridges which are observed in this region can be attributed to mechanical damage (resulting from the pretreatment), extending deeper than the width of the space-charge region, and hence leading to recombination in the diffusion layer. Indeed, GaP has poor absorption characteristics so that the light penetrates the crystal quite deeply[69]. This interpretation is supported by the observation that when measuring the local photocurrent by laser-scanning of Si, which also has poor absorption characteristics, the photocurrent onset region allows us to visualize structures with enhanced surface recombination, whereas in the

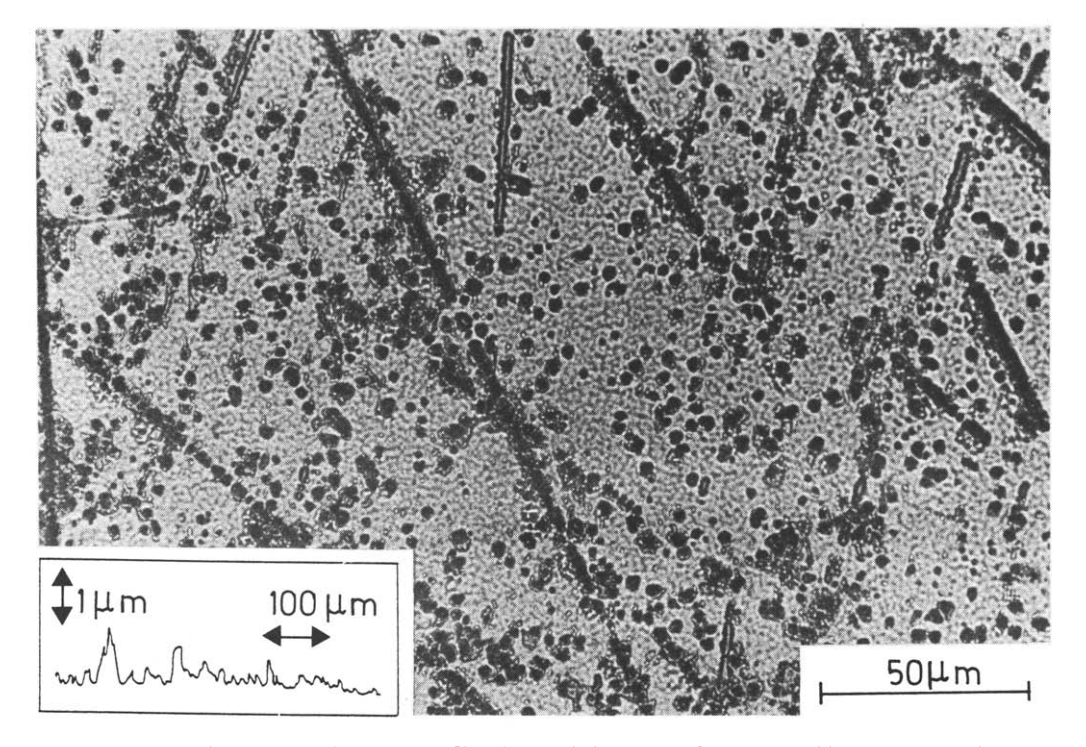


Fig. 5. Photomicrograph and surface profile of an n-GaP (111)-surface after etching during 10 min at $i = 0.3 \text{ mA cm}^{-2}$ under full light intensity in aqueous KOH (pH = 13).

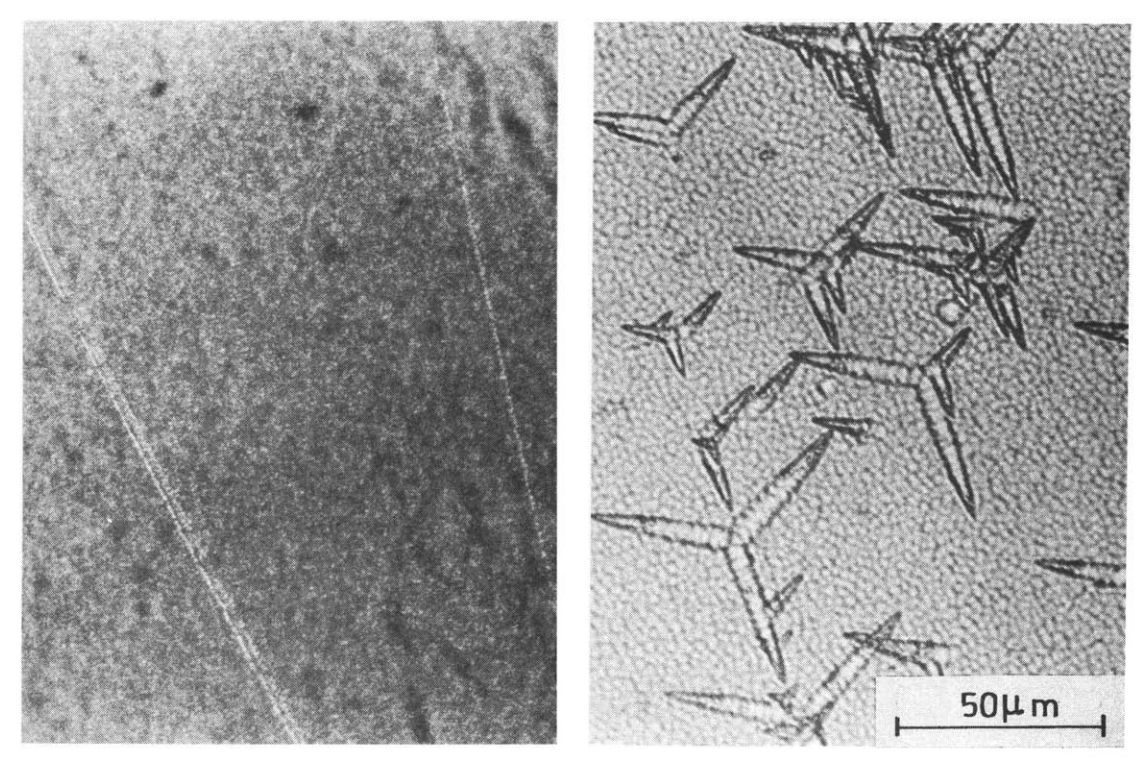


Fig. 6. Photomicrograph at n-GaP after etching at $V=+1.6\,\mathrm{V}$ (vs. sce) in aqueous KOH (pH = 13). Left: (100)-face, light intensity = 10% of full value, etching time = 15 min. Right: (111)-face, light intensity = 15% of full value, etching time = 1 h.

photocurrent plateau diffusion layer recombination determines the local photocurrent[70]. In the case of GaAs, in which the light is absorbed in a very thin layer underneath the surface, recombination centers are not visualized by the scanning-laser technique when polarizing the anode in the plateau region [71–73]. The difference in morphology between the (III)- and (111)-faces can be interpreted on the basis of a difference in hole capture reactivity, as mentioned earlier, so that holes at the (111)-face have more chance to move parallel to the surface and hence to react selectively at reactive sites[29]. The typical morphology of the starlike pits is not fully understood yet, but the fact that this morphology only develops at photoanodically etched n-type surfaces indicates a possible effect of non-uniform hole flow towards the surface. Similar etch pits have been reported for n-GaAs[57, 58, 74], without satisfactory explanation either. The fact that in the present case, the (100)-face shows a morphology similar to that of the (III)-face, can be attributed to the comparable reactivity of both faces.

3.1.2. (Photo) anodic etching of GaP in acid solutions. Neglecting the small contribution of conduction bands electrons (see Section 3.1.1.), the stoichiometry of the six-equivalent anodic oxidation of GaP at pH = 1 can be written as

$$GaP + 6h^{+} + 3H_{2}O \rightarrow Ga^{3+} + H_{3}PO_{3} + 3H^{+}$$
. (3)

The current-potential curve of a p-GaP electrode in aqueous H_2SO_4 solutions (pH = 1) is shown in Fig. 7. A passivation effect is observed at high anodic current densities, as has been reported before by Madou *et al.*

[75]. In the rising part of the i-V curve (region I, Fig. 7), the etching leads to the formation of pits with a geometry similar to that revealed in alkaline solutions, but is less selective than in alkaline solutions, ie much more material (up to five times more) has to be removed to develop the pits. As in alkaline solutions, the (111)-face was found to be more selectively etched than the (100)- and (III)-faces. The same interpretations hold as in the case of pH = 13. The reduced selectivity in acid solutions might be attributed to a higher mobility of the surface decomposition intermediates [such as X_1^+ , equation (2)], which would counteract the local differences in the hole capture rate of an X₀ site [see equation (2)]. Lingier et al. [21, 76, 77] showed that the mobile intermediate X₁ can be neutralized by water (or by OH⁻ in alkaline solutions) to form the immobile intermediate X_1 -OH:

$$X_1^+ + H_2O \Longrightarrow X_1\text{-OH} + H^+.$$
 (4)

From equation (4), the concentration of mobile intermediates is expected to increase with decreasing pH. From stabilization and excitation experiments at the n-GaP anode, however, it has been concluded that most of the decomposition intermediates of GaP are immobile even in acidic solutions[50, 78–81], which seems to contradict the proposed explanation.

At potentials corresponding to the passivation region II (Fig. 7), etching of p-GaP reveals a few scratches only, no distinct pits being observed. In contrast to alkaline solutions, a steady state situation in which the rates of generation and further reaction of the intermediates would be equal and in which the

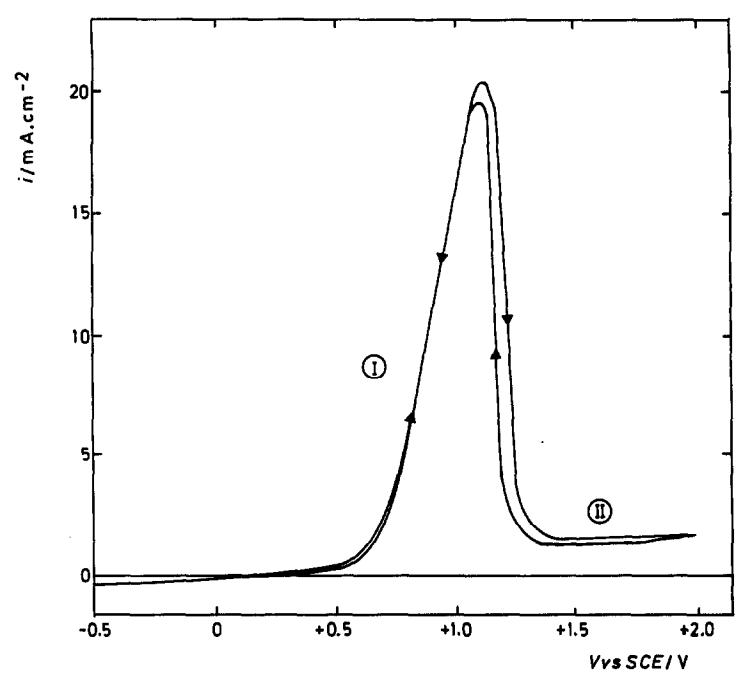


Fig. 7. Current density-potential curve at a dark (100) p-GaP rotating electrode in aqueous H_2SO_4 (pH = 1). Rotation rate = 20 s⁻¹, scan rate = 1 mV s⁻¹.

plateau current density would be determined by the kinetics of a chemical step, is not to be expected here. Instead, in acidic solutions at sufficiently high anodic current densities, an oxidation product of GaP will be formed which is thermodynamically insoluble, resulting in a passivating product layer. This product layer might be an oxide with a complex Ga-P-O composition[82, 83]. The current density flowing under these circumstances depends on the physical and chemical characteristics of this layer, which were not studied in detail. The scratches observed might be

attributed to the possible bad adherence of the layer at damaged surface sites, allowing local enhanced dissolution.

At n-GaP, passivation only occurs at high illumination levels of the surface (Fig. 8). At low light intensities, the i-V characteristics are similar to those at low light intensities in alkaline solutions (see Fig. 2). Results analogous to those in alkaline solutions were obtained as far as the surface morphology after etching is concerned, consisting of hillocks and ridges in the photocurrent onset region I and of microrough

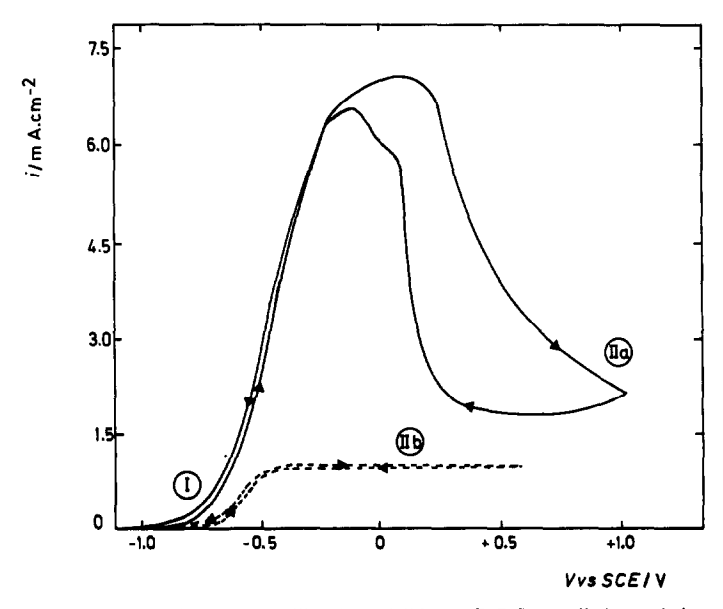


Fig. 8. Current density-potential curve at an illuminated (100) n-GaP flow-cell electrode in aqueous H₂SO₄ (pH = 1). Flow rate = 50 ml h⁻¹, scan rate = 5 mV s⁻¹. (——) Full light intensity; (---) 15% of full light intensity.

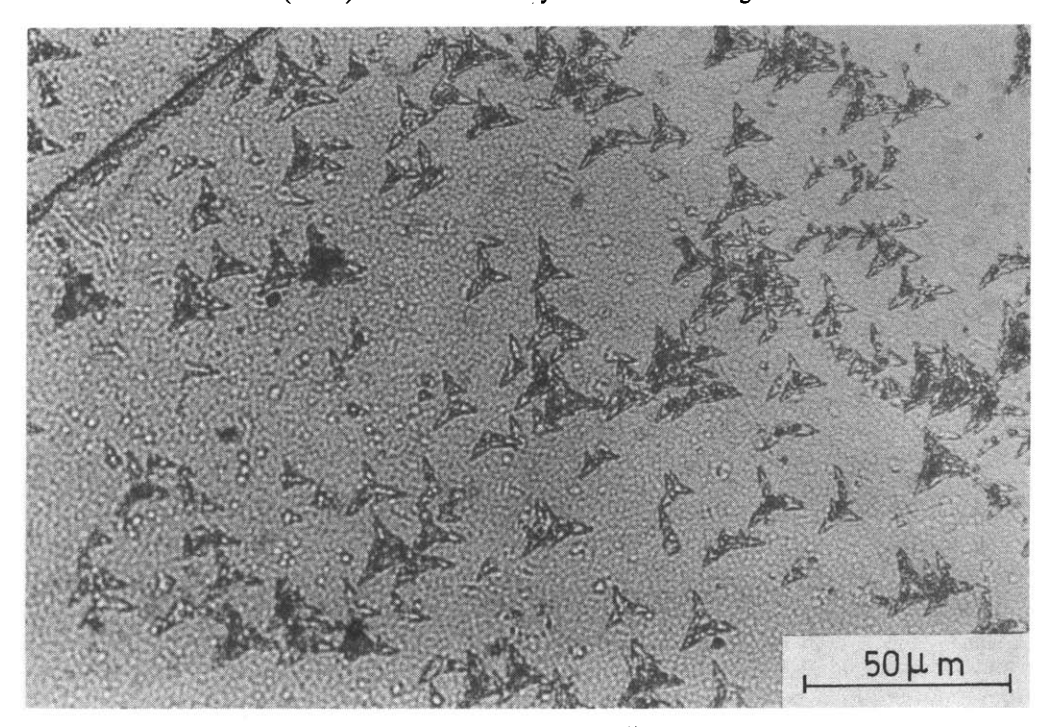


Fig. 9. Photomicrograph of an n-GaP (111)-face after etching during 50 min at $V=+1.6\,\mathrm{V}$ (vs. sce) in aqueous $\mathrm{H_2SO_4}$ (pH = 1). Light intensity = 15% of full value.

(100)- and (III)-faces in the photocurrent plateau region IIb, whereas at the (111)-face isosceles triangular etch pits are developed in the latter region (see Fig. 9). The fact that the latter are less sharply shaped than those developed in alkaline

solutions may again indicate that the etching in acidic solutions proceeds less selectively than in alkaline solutions.

When the n-GaP single crystals are photoanodically etched in the passivation region IIa (Fig. 8) (at full

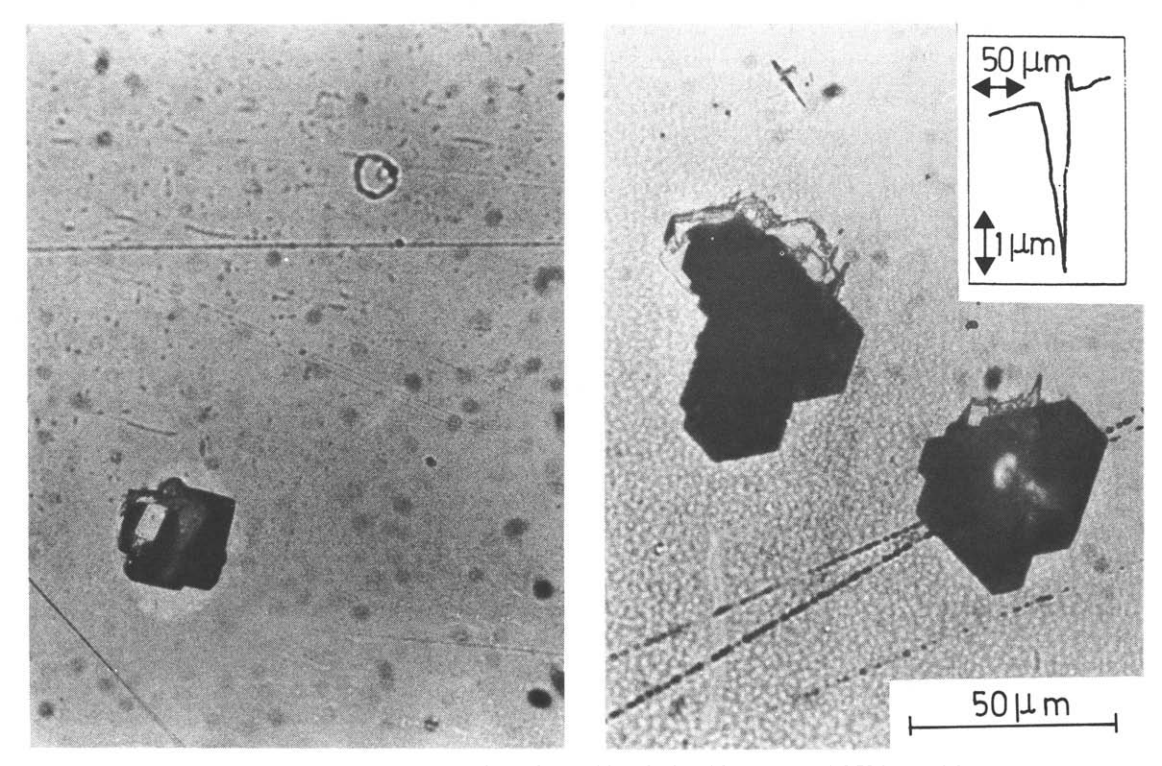


Fig. 10. Photomicrograph of an n-GaP surface after etching during 1 h at V = +1.9 V (vs. sce) in aqueous H_2SO_4 (pH = 1) at full light intensity. Left: (100)-face. Right: (III)-face. Insert: pit profile.

light intensity), large-size etch pits are formed besides a few scratches (Fig. 10). The edges of these pits form angles depending on the crystal face, ie angles of about 90° at the (100)-face and of about 120° at the (III)- and (111)-faces, hence obviously reflecting the symmetry of the crystal lattice along the axis concerned. The reason for the development of these pits and for the fact that they develop at n-type crystals only is not fully understood, but is probably related to the physical characteristics of the passivating layer such as the rates of electron and ion transport through this layer and the optical absorption, which are unknown at present.

The occurrence of a passivation phenomenon in acid solutions may explain why in alkaline solutions, the role of OH⁻ ions is not taken over by H₂O molecules when the dissolution rate reaches the OH⁻ diffusion limit [cf. reaction equation (1) and equation (3)]. Indeed, one would expect that when the surface is depleted of OH⁻ ions due to their diffusion-limited consumption, H₂O molecules would take over their role as the nucleophilic agent since they are able to act this way at low pH-values [see equation (4)]. However, comparison of Fig. 1 with Fig. 7 or of Fig. 2 with Fig. 8 shows that the OH⁻ diffusion limit is well above the passivation peak and hence suggests that OH⁻ ions are essential in order to avoid the formation of a passivating layer at relatively high current densities.

For the sake of completeness it is interesting to remark that in the case of GaAs also, a passivation effect has been observed in acidic solutions[84, 85], whereas OH- diffusion limitation of the anodic current density has been observed in alkaline solutions [24, 86]. Although a systematic comparative study of the kinetics of the anodic dissolution reaction and the morphology of the etched surface has not been carried out for GaAs and InP, it seems that several of the conclusions drawn for GaP also hold for these materials. For example, it is found that photoanodic etching of GaAs and InP in the photocurrent onset region leads to very selective etching with the formation of etch hillocks, whereas photoanodic etching in the photocurrent plateau region is often found to be poorly selective, leading to the development of sporadic etch pits in certain cases[57, 71, 87–89].

3.1.3. (Photo)anodic etching of GaP: general considerations. From the above results, it follows that the morphology of the (photo)anodically etched GaP surface is determined by the kinetics of the anodic dissolution reaction. Etching at a diffusionlimited rate leads to uniformly flat surfaces, whereas in all other cases etch figures are developed as a result of local differences in the reaction rate. An important difference is observed between p- and n-type crystals. For p-GaP the holes are spread out at the surface in a quasi-equilibrium cloud, so that local differences in the anodic reaction rate are due to differences in hole capture rate. For n-GaP, the holes are the minority carriers and their reaction rate at the surface is mainly determined by their availability. In this case, inhomogeneities in the space-charge layer and recombination processes cause differences in the hole supply rate and hence in the etch rate. In the presence of a passivating surface layer, the physical and chemical properties of this layer may furthermore determine the surface morphology.

The selectivity of the process is determined by the ratio of the etch rate at defect vs. normal surface sites. The latter was assumed to be the lowest at the (111)-face, accounting for the high selectivity of this face relative to that at the (III)- and the (100)-face.

The concepts developed here will appear to be important in the interpretation of the surface morphology and etching selectivity of open-circuit etching processes.

3.2. Electroless etching

The open-circuit etching of [111]-oriented GaP crystals in alkaline K_3 Fe(CN)₆ solutions (pH = 13) was shown to proceed via an electroless etching mechanism[46]: holes are injected into the valence band of GaP by Fe(CN)₆³⁻ ions (as appears from the fact that Fe(CN)₆³⁻ enhances the cathodic dark current at the p-GaP electrode considerably), and are consumed in the dissolution reaction (1). Hence, two partial currents are flowing under open-circuit conditions or at rest potential which cancel each other electrically, but not chemically:

GaP + 6h⁺ + 11OH⁻

$$\rightarrow$$
 GaO₃³⁻ + HPO₃²⁻ + 5H₂O (1)
6[Fe(CN)₆³⁻ \rightarrow Fe(CN₆⁴⁻ + h⁺] (5)

GaP + 6Fe(CN)₆³⁻ + 11OH⁻

$$\rightarrow$$
 GaO₃³⁻ + HPO₃²⁻ + 6Fe(CN)₆⁴⁻ + 5H₂O. (6)

A typical feature of a purely electroless etch mechanism is the lack of etching when the electrode is polarized cathodically, since then the holes, injected by the oxidizing agent, migrate into the semiconductor so that reaction (1) cannot occur. This indeed appears to be the case with Fe(CN)₆³ at GaP. A detailed discussion of the electrochemistry and of the etching kinetics at the GaP/Fe(CN)₆³⁻ interface has been presented in Ref.[46] and will not be repeated here. However, in view of the discussion of the surface morphology, it is necessary to recall certain results on the etching kinetics. From flow-cell measurements, the etch rate was found to be controlled by the hole injection step at the (111)-face (so-called kinetic control) and by diffusion, either of Fe(CN)₆³ (for $Fe(CN)_6^{3-}$ concentrations lower than 0.3 mol 1^{-1}) or of OH^{-1} (for $Fe(CN)_6^{3-1}$ concentrations higher than 0.3 mol 1^{-1}) at the (III)-face, implying that the actual charge transfer step is faster at the (III)-face. This difference has been related to the observed difference in valence band edge position, resulting in a better overlap with the empty redox levels at the (III)-face than at the (111)-face[46].

As to the morphology of the GaP surfaces etched in alkaline K_3 Fe(CN)₆ solutions (pH = 13), it was found that more or less equilateral triangular etch pits are developed at the (111)-face (pits of 1-2 μ m deep appear after removal of a 10 μ m layer), whereas the (III)-face is etched homogeneously[46]. However, we recently found that also at the (III)-face of p-GaP, equilateral triangular etch pits can be developed, but only at Fe(CN)₆⁻ concentrations below 0.3 mol 1⁻¹ and after a very long etching time (>48 h). Furthermore it is important to note that this effect does not occur at n-type crystals.

Face	Туре	Fe(CN) ₆ ³ -concentration	Schematic i-V behaviour	Rate-determining step	Surface morphology
(111)	р	$c \leqslant 1 \mod 1^{-1}$	Fig. 11a	Injection of h+, kinetically controlled	Equilateral triangular pits
	n	$c\leqslant 1 \bmod 1^{-1}$	Fig. 11c	Injection of h ⁺ , kinetically controlled	Equilateral triangular pits
(III)	р	$c < 0.3 \text{mol} 1^{-1}$	Fig. 11a	Diffusion of Fe(CN) ₆ ³	Equilateral triangular pits, only observed after a long etching time
		$0.3 \leqslant c \leqslant 1 \bmod 1^{-1}$	Fig. 11b	Diffusion of OH-	Homogeneously flat
	n	$c < 0.3 \mathrm{mol}\mathrm{l}^{-1}$	Fig. 11c	Diffusion of Fe(CN) ₆ ³⁻	Homogeneously flat
		$0.3 \leqslant c \leqslant 1 \bmod 1^{-1}$	Fig. 11d	Diffusion of OH	Homogeneously flat

For the sake of clarity and in view of the following discussion, the results on electroless etching by Fe(CN)₆⁻ are summarized in Table 1.

The morphology of the etched surfaces, including the anomalous effect at (III) p-GaP, can be understood on the basis of the electroless mechanism and hence from electrochemical principles. For this, we assume that the two partial electrochemical reactions of the electroless process do not necessarily take place at the same sites, a concept which is quite familiar in metallic corrosion. Furthermore, since only the anodic partial current involves dissolution of the semiconductor, it is important to realize that local differences in the anodic partial current density only are reflected in the surface morphology. In p-GaP the holes, being the majority carriers, are spread out at the surface in a quasi-equilibrium cloud, as already stated in Section 3.1. The anodic partial reaction rate at a given site is then determined by the local hole capture reactivity, which hence determines the surface morphology, except when the anodic partial reaction rate is limited by OH- diffusion. In the latter case, the anodic partial reaction rate is the same over the whole surface. The situation for n-GaP, however, is quite different. Here, the holes are the minority carriers and do not constitute a quasi-equilibrium cloud at the surface since they can be assumed to be very rapidly captured in surface bonds (see Section 3.1 and Ref.[29]). For n-type crystals, it is the availability of holes at the surface which determines the anodic partial reaction rate and hence the surface morphology. For an electroless etching process, holes are made available by injection from the solution [reaction (5)], so that for n-GaP the anodic partial reaction (1) is expected to take place at (nearly) the same sites at which the holes are injected by $Fe(CN)_6^{3-}$. The morphology then reflects local differences in the hole injection rate. When either the injection rate is limited by Fe(CN)₆³ diffusion or the anodic partial reaction rate is limited by OH- diffusion, the anodic partial current density is the same all over the surface.

With these reflections in mind, the interpretation of the morphology of the GaP surfaces etched in alkaline K_3 Fe(CN)₆ solutions is straightforward. At the (111)-face, the overall etch rate is kinetically controlled. For (111) p-GaP, the i-V curves are schematically shown in Fig. 11a (the shape of the different i-V curves shown in Fig. 11 and especially the potential dependence of the hole injection rate, related to band edge shifts, is discussed in detail in Ref. [46]); the situation at the rest potential V_r corresponds to the rising part of the anodic partial current density. Etch pits are formed due to local differences in hole capture reactivity, analogously to the anodic etching of p-GaP in the rising part of the i-V curve (Fig. 1, region I). For (111) n-GaP, the i-V behaviour is schematically represented in Fig. 11c. Etch pits are formed at sites with a locally enhanced injection rate of holes, due to a locally higher position of the valence band edge (dislocation sites). In this case, the situation is analogous to the photoanodic etching of n-GaP in the photocurrent plateau (Fig. 2, region IIb) in this respect, that the morphology is determined by local differences in the availability of holes at the surface. An important difference however is, that the holes are not created by photons inside the semiconductor but are injected from the solution. This explains why in the case of electroless etching, no isosceles triangular etch pits in starlike configurations are observed, since—as assumed in Section 3.1—this specific geometry is a consequence of the inhomogeneous flow of holes through the space-charge layer.

Let us now consider the (III)-face. For (III) p-GaP and at low $Fe(CN)_6^{3-}$ concentrations (<0.3 mol l⁻¹) the overall etch rate is determined by diffusion of $Fe(CN)_6^{3-}$. The situation at the rest potential V_r then corresponds to the rising part of the anodic partial current density curve (Fig. 11a) and etch pits are again formed as a result of local differences in hole capture reactivity. The fact that these pits are only visible after a long etching time may be ascribed to the low etch rate at these low concentrations on the

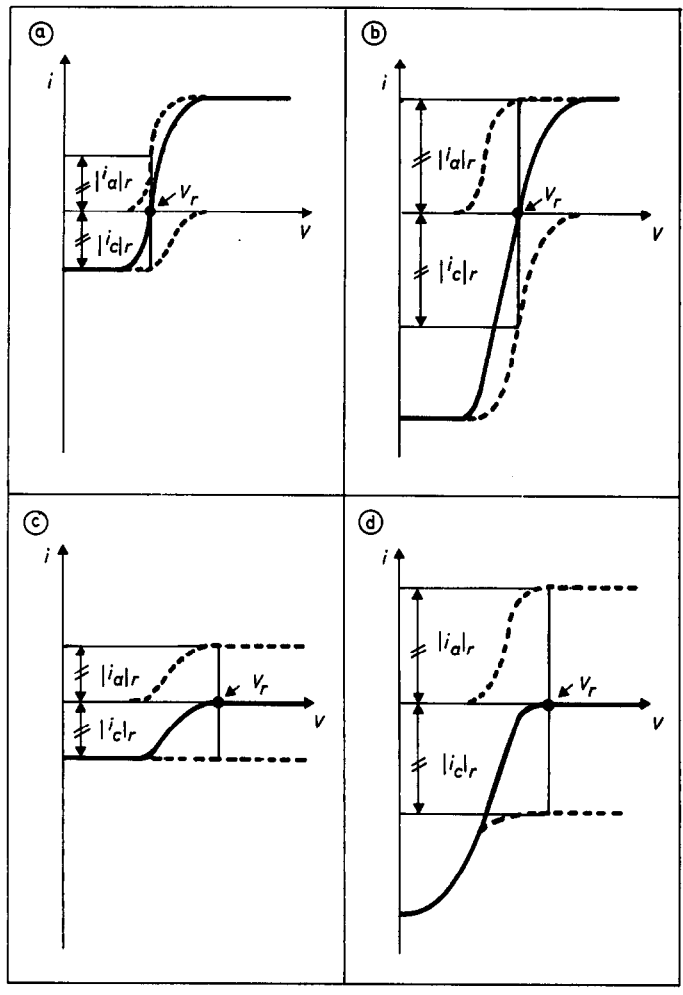


Fig. 11. Schematic representation of the i-V behaviour of GaP in alkaline Fe(CN) $_6^3$ solutions. (a) and (b): p-GaP. (c) and (d): n-GaP. (——) Overall current density; (——) partial current densities.

one hand, and to the low selectivity of the (III)-face as discussed in Section 3.1 on the other hand. At high Fe(CN)₆³ concentrations, the overall etch rate at p-GaP is determined by the diffusion rate of OH-. The situation at the rest potential V, then corresponds to the plateau region of the anodic partial current density (Fig. 11b), resulting in a homogeneously flat surface, similarly to the case of the anodic etching of p-GaP in the diffusion-limited regime (Fig. 1, region II). For (III) n-GaP at low $Fe(CN)_6^{3-}$ concentrations $(<0.3 \text{ mol } l^{-1})$, the overall etch rate is determined by $Fe(CN)_6^{3-}$ diffusion. The i-V behaviour is shown schematically in Fig. 11c; the etched surface is homogeneously flat since the hole supply, ie the hole injection rate, is the same all over the surface. At high $Fe(CN)_6^{3-}$ concentrations (>0.3 mol l⁻¹) the overall etch rate is limited by the OH- diffusion rate. The schematic i-V curves are shown in Fig. 11d, in which the anodic partial current density reaches its OHdiffusion limit. A flat surface is formed, analogously to the diffusion-limited photoanodically etched surfaces (Fig. 2, region IIa).

The interpretation of the morphology of electroless etch processes at GaP is hence analogous to that proposed for the photoanodic etching processes, be it that in the present case, the potential is not applied by an external source but is imposed as a rest potential by addition of Fe(CN)₆³ to the solution.

The open-circuit etching of GaAs in K₃Fe(CN)₆ solutions also proceeds via an electroless mechanism [18, 86, 90]. In this case, it was found that etch pits develop at both n- and p-GaAs when the etching is diffusion-limited through the cathodic partial reaction [90]. Furthermore, also in the profile etching of GaAs in alkaline K₃Fe(CN)₆ solutions, a difference is observed depending on whether the process is diffusionlimited either by Fe(CN)₆³ or by OH⁻, independently of the semiconductor type[90]. Whereas a rounded profile, typical for diffusion-limited etching, is observed at the resist edge when the etch rate is limited by OH diffusion, a faceted (anisotropic) profile is found when Fe(CN)₆³ diffusion determines the etch rate. An interpretation based upon galvanic element formation between different crystal planes has been given and is hence in some way analogous to our interpretation for the formation of etch pits at p-GaP when etched with a Fe(CN)₆³⁻ diffusion-limited rate, since in both cases a spatial separation of anodic and cathodic regions is assumed. The fact that at GaAs, in contrast to GaP, a distinction between diffusion

limitation by the cathodic partial reaction and diffusion limitation by the anodic partial reaction is observed also at n-type crystals, may be due to the higher hole mobility in GaAs so that in that case, holes injected at a diffusion-limited rate may be able to move parallel to the surface before being captured selectively. Other electroless etchants for GaP and GaAs include acidic Ce⁴⁺ and Fe³⁺ solutions [20, 91–93].

3.3. Chemical etching

The etching of GaP single crystals in acidic Br_2 solutions proceeds via a chemical mechanism, as was concluded from the facts that cathodic polarization does not impede the etching of p-GaP and that Br_2 is not able to inject holes into the valence band of GaP [45]. From combined etching and electrochemical experiments, the stoichiometry of the reaction has been identified as

GaP + 3Br₂ + 3H₂O

$$\rightarrow$$
 Ga³⁺ + H₃PO₃ + 3H⁺ + 6Br⁻. (7)

The rate of the etching process was found to depend on the crystal orientation, being kinetically controlled at the (111)-face and limited by the diffusion rate of Br₂ towards the GaP surface at the (III)-face. This difference in reactivity between both polar faces with respect to the electrophilic reactant Br₂ can be explained by the higher electron density at the (III)-face, due to the different orientation of the Ga-P surface dipole[12, 62].

As to the morphology of the etched surfaces, it was found that the (III)-face is always etched homogeneously flat, whereas more or less equilateral triangular etch pits are formed at the (111)-face. No difference is observed between n- and p-type crystals. This may be explained as follows. Since etching does not involve holes, considerations pertaining to free charge carriers of the semiconductor are irrelevant. At the (III)-face, the etch rate is determined by diffusion of Br, and is hence equal at all sites (homogeneous etching). At the (111)-face, where the etch rate is determined by the surface reaction (7) itself, sites with a higher reactivity (defect sites) will be etched faster and will hence form etch pits. The selectivity of the etching at the (111)-face is found to be about 10 times higher than that for the anodic and electroless etching processes.

Electrochemical measurements not only enabled us to establish that the etching mechanism of GaP in Br₂ is a chemical one, but also led us to conclude that the mechanism is not a concerted one but involves consecutive steps, as follows from the observation of electron-injection by intermediates[45]. This phenomenon is very similar to that observed under anodic etching of GaP in indifferent solutions. This explains the occurrence of a mixed anodic-chemical dissolution mechanism observed at the p-GaP anode in the presence of Br₂, in which the competitive chemical and anodic steps are coupled through these decomposition intermediates.

A chemical etching mechanism involving consecutive steps has also been reported for the etching of GaAs by Br_2 , H_2O_2 and $OBr^-[94-96]$. Other chemical etchants for GaAs include $I_2[97]$ and $OCl^-[98]$. The

etching of InP in HCl, HBr and Br₂ solutions was also shown to be chemical[99, 100]; in the case of HCl and HBr, it was demonstrated that the etching proceeds with undissociated molecules only. The etching of InP by HCl or HBr is non-oxidative, so that in these cases, electron-injecting oxidation intermediates of InP are not formed, as demonstrated for HCl etching[101].

3.4. Photoetching

Hypobromite has been found to be an efficient photoetching reactant for GaP[44]. This may be understood on an electrochemical basis. Indeed, when registering i-V curves at n- and p-GaP under illumination in aqueous KOH (pH = 13) solution, it is found that, whereas the anodic partial current density is not influenced by the presence of OBr-, the cathodic partial current density is significantly shifted towards more positive potentials when adding OBrto the indifferent electrolyte. As a result, in alkaline OBr - solutions under illumination, the two compensating partial currents at rest potential are substantially higher than in solutions without OBr-. Referring to Fig. 12, which contains a schematic representation of the situation, the procedure for determining experimentally the absolute value of these partial current densities can be explained as follows. The potential of the GaP electrode in contact with the hypobromite solution is adjusted to the value at which the net current density is zero under illumination; then, keeping the potential constant at that value, the current density right after switching off the light is measured (in practice, a chopper is used). From Fig. 12 it follows that in this way, one measures one

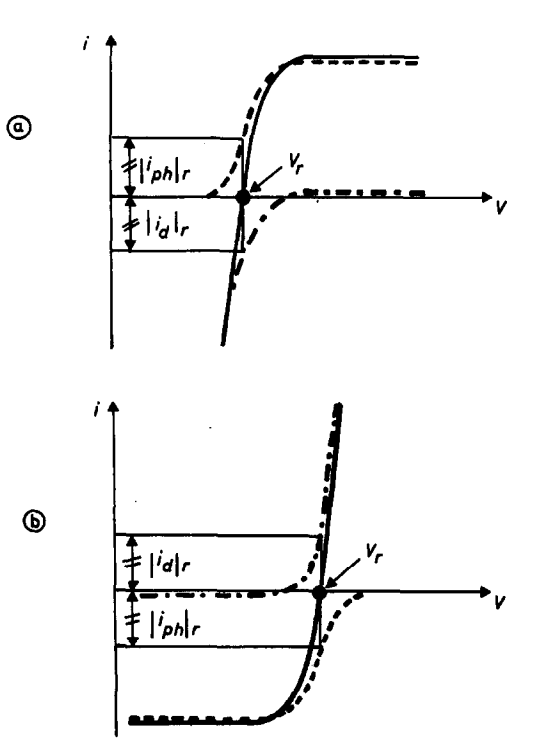


Fig. 12. Schematic representation of the i-V behaviour of illuminated GaP in alkaline OBr⁻ solutions. (a) n-GaP (b) p-GaP (——) Total current density under illumination; (——) dark current density; (——) photocurrent density.

of the equal and opposite partial current densities under illumination, the cathodic one for n-type and the anodic one for p-type electrodes. Taking into account the fact that the anodic oxidation of GaP is six-equivalent, the absolute value of the partial current densities at rest potential under illumination can be converted into the electrochemical etch rate under illumination at rest potential. The values thus obtained appear to be in good agreement with those for the photoetch rate of GaP in OBr- solutions (ie the etch rate under illumination minus that in darkness, both at rest potential), determined analytically from flow-cell experiments. This indicates that the photoetching proceeds via a simple electrochemical mechanism involving two corresponding partial currents, ie the anodic oxidation of GaP [reaction (1)], and the cathodic reduction of OBr - according to reactions (8) and (9) (current doubling at p-GaP):

$$OBr^{-} + e^{-} + H_{2}O \rightarrow Br' + 2OH^{-}$$
 (8)

$$Br^* \rightarrow Br^- + h^+$$
. (9

The difference with respect to an electroless mechanism is that here, illumination is necessary, since the reduction of the oxidizing agent—or actually its first step—proceeds over the conduction band. The overall reaction may hence be written as

$$GaP + 3OBr^- + 5OH^-$$

$$\xrightarrow{h\nu} GaO_3^{3-} + HPO_3^{2-} + 3Br^{-} + 2H_2O. \quad (10)$$

As far as the morphology of the photoetched (111)and (III)-surfaces is concerned, a remarkable effect is observed: etch hillocks develop on n-GaP (similar to those formed by photoanodic etching of n-GaP in the onset region of the photocurrent-potential curve) whereas etch pits are formed on p-GaP (similar to those formed by anodic etching of p-GaP in the rising part of the i-V curve)[29]. As in the case of electroless etching, it is again assumed that on the microscale, the two partial reactions under consideration do not necessarily take place at the same sites. The morphology then reflects local differences in the anodic partial reaction rate, which are due to local differences in the hole supply rate for n-GaP and to local differences in hole capture reactivity for p-GaP. It is interesting to note here that in earlier work[44], we were indeed led to assume that the steady-state concentration of holes is much larger at the p-GaP surface than at the n-GaP surface, in order to explain an anomalous dark etching effect at n-GaP in alkaline OBr - solutions (induced by the photoetching effect of OBr-) and its absence at p-GaP. This difference also accounts for the difference in surface morphology between photoetched n- and p-GaP crystals. Indeed, at n-GaP, the anodic partial reaction proceeds by the minority carriers. The situation at rest potential corresponds to the onset of the photocurrent-potential curve (see Fig. 12), in which recombination processes determine the availability of holes and hence the value of the current density. The hillocks, formed by photoetching, then correspond to sites of enhanced recombination rate (dislocation sites, damaged sites). In the case of p-GaP, however, the holes being the majority carriers, local enhanced recombination indeed leads to a local decrease of the

cathodic partial current density (and hence to a decrease of the overall etch rate) but does not significantly influence the local anodic partial current. The situation is in this case analogous to the anodic etching of p-GaP in the rising part of the i-V curve (see also Fig. 12): the holes constitute a quasiequilibrium cloud at the surface, so that sites with an enhanced reactivity for hole capture lead to the formation of etch pits.

For the photoetching of InP in acidic Fe³⁺ solutions, it has also been demonstrated recently that the mechanism is a purely electrochemical one, involving two compensating partial currents[102]. Morphological data are however as yet not available. In the case of GaAs photoetching in CrO₃-HF solutions, etch hillocks are formed both on n- and p-type crystals[36, 37]. However, hillocks are formed even in darkness, which has been explained by a rather complex electroless etching model, where passivation by adsorption of CrO₃ reduction intermediates and depassivation via decomposition intermediates play a crucial role[103-105]. The CrO₃-HF etch solution is very sensitive for revealing defects at GaAs and even more so at InP crystals[106]. A similar mechanism appears to hold in the case of the photoetching of GaAs in CrO₃-HCl[59].

The fact that the anodic and cathodic partial reactions do not necessarily take place at the same site is even more obvious in laser-photoetching. There the illuminated surface area is very small in comparison to the dark area, which may lead to a strong enhancement of the etch rate under illumination due to galvanic element formation[107–109].

4. CONCLUSIONS

This investigation shows that (photo)electrochemistry forms a powerful tool to investigate wet etching processes at III-V semiconductors. The strategy of combining kinetic, morphological and electrochemical studies enables one not only to unravel the mechanisms of the different etching processes under consideration, but also to obtain fundamental insight into the origin of the surface morphology of the etched surfaces. In the case of electroless and photoetching, the interpretation of the kinetic and morphological data is analogous to that of anodic etching, with this difference that the electrode is forced at a given point in the anodic partial current-potential curve not by an external potential source, but by the illumination and/or the oxidizing agent, imposing a rest potential.

Several concepts have appeared to be important in the interpretation of the surface morphology. Firstly, diffusion limitation of the dissolution reaction, ie of the anodic (partial) reaction or of the chemical reaction, leads to homogeneously flat surfaces, whereas in all other cases, local differences in the surface reaction rate, due to whatever cause, lead to specific etch patterns. Secondly, for etching processes involving an electrochemical mechanism, the semiconductor type plays a distinctive role, caused by the fact that the holes constitute a quasi-equilibrium cloud at the p-GaP surface, in contrast to n-GaP. A further concept, essential for electroless and photoetching processes, is that the two partial currents

do not necessarily flow at the same site. Finally, the differences in etch selectivity between different crystal faces have been attributed to differences in etch rate of normal surface sites, assuming that the dependence of the reactivity on crystal orientation at defect sites is negligible.

Acknowledgements-The authors are indebted to K. Strubbe, I. Vermeir and Ph. Verpoort for their cooperation to part of this work and to L. Van Meirhaeghe for performing the Talystep measurements. The financial support of the I.I.K.W. (Inter-University Institute for Nuclear Sciences, Belgium) is gratefully acknowledged. H. H. G. is a research assistant of the N.F.W.O. (National Fund for Scientific Research, Belgium).

REFERENCES

- 1. M. Datta and L. T. Romankiw, J. electrochem. Soc. 136, 2850 (1989).
- 2. H. Beneking, J. electrochem. Soc. 136, 2680 (1989).
- 3. A. Ramam, S. Kapoor, S. Prabhakar, R. Gulati and I. Chandra, J. electrochem. Soc. 136, 2405 (1989).
- 4. T. Uragaki, H. Yamanaka and M. Inoue, J. electrochem. Soc. 123, 580 (1976).
- 5. S. Mottet and L. Henry, Electron. Lett. 19, 919 (1983).
- 6. D. Moutonnet, Mater. Lett. 6, 183 (1988).
- 7. R. M. Lum, A. M. Glass, F. W. Ostermayer Jr., P. A. Kohl, A. A. Bailman and R. A. Logan, J. appl. Phys. **57,** 39 (1985).
- 8. F. W. Ostermayer Jr., P. A. Kohl and R. H. Burton, Appl. Phys. Lett. 43, 642 (1983).
- 9. G. A. Rozgonyi, A. R. Von Neida, T. Iizuka and S. E.
- Haszko, J. appl. Phys. 43, 3141 (1972). 10. W. R. Wagner, L. I. Greene and L. I. Koszi, J. electrochem. Soc. 128, 1091 (1981).
- 11. G. Wagner and V. Gottschalch, Cryst. Res. Technol. 23, 59 (1988).
- 12. H. C. Gatos and M. C. Lavine: in Progress in Semiconductors, Vol. 9, (Edited by A. F. Gibson and R. E. Burgess) p. 29. Temple Press Books, London (1965).
- 13. Y. Tarui, Y. Komiya and Y. Harada, J. electrochem. Soc. 118, 118 (1971).
- 14. F. A. Thiel and L. R. Barns, J. electrochem. Soc. 126, 1272 (1979).
- 15. W. Kern and G. L. Schnable, in The Chemistry of the Semiconductor Industry, (Edited by S. J. Moss and A. Ledwith) p. 229. Blackie & Son, London (1987).
- 16. D. V. Morgan and K. Board, An Introduction to Semiconductor Microtechnology, p. 34. J. Wiley & Son, Chichester (1990).
- 17. D. L. Flamm and J. A. Mucha, in The Chemistry of the Semiconductor Industry, (Edited by S. J. Moss and A. Ledwith) p. 343. Blackie & Son, London (1987).
- 18. H. Gerischer, Ber. Bunsenges. phys. Chem. 69, 578 (1965).
- 19. H. Gerischer and I. Willem-Mattes, Z. Phys. Chem. NF 64, 187 (1969)
- 20. R. Memming and G. Schwandt, Electrochim. Acta 13, 1299 (1968).
- 21. W. P. Gomes, S. Lingier and D. Vanmaekelbergh, J. electroanal. Chem. 269, 237 (1989).
- 22. D. Vanmaekelbergh and W. P. Gomes, J. phys. Chem. 94, 1571 (1990).
- 23. J. J. Kelly and P. H. L. Notten, J. electrochem. Soc. **130,** 2452 (1983).
- 24. F. Decker, Electrochim. Acta 30, 301 (1985).
- 25. P. Allongue and H. Cachet, Electrochim. Acta 33, 79 (1988)
- 26. Y. Nakato, A. Tsumura and H. Tsubomura, J. electrochem. Soc. 127, 1502 (1980).

- 27. R. Sukale, P. Janietz, R. Landsberg and H. Kaukel, Z. Phys. Chem. 266, 897 (1985).
- 28. K. W. Frese Jr., M. J. Madou and S. R. Morrison, J. electrochem. Soc. 128, 1527 (1981).
- 29. H. H. Goossens and W. P. Gomes, J. electrochem. Soc. 138, 1696 (1991).
- 30. H. Gerischer and I. Mattes, Z. Phys. Chem. NF 49, 112 (1966).
- 31. H. Gerischer and W. Mindt, Electrochim. Acta 13, 1329 (1968).
- 32. H. Gerischer, Surf. Sci. 18, 97 (1969).
- 33. F. Kuhn-Kuhnenfeld, J. electrochem. Soc. 119, 1063 (1972).
- 34. L. Blok, J. Cryst. Growth 31, 250 (1975).
- 35. T. Saitoh, S. Matsubara and S. Minagawa, J. electrochem. Soc. 122, 670 (1975).
- 36. J. L. Weyher and J. van de Ven, J. Physique 43, C5-313 (1982).
- 37. J. L. Weyher and J. van de Ven, J. Cryst. Growth 63, 285 (1983).
- 38. D. V. Podlesnik, H. H. Gielgen and R. M. Osgood Jr, Appl. Phys. Lett. 45, 563 (1984).
- 39. R. D. Rauh and R. A. LeLievre, J. electrochem. Soc. 132, 2811 (1985).
- 40. D. Moutonnet, Mater. Lett. 6, 433 (1988).
- 41. J. J. Kelly, J. E. A. M. van den Meerakker and P. H. L. Notten, in Grundlagen von Elektrodenreaktionen, (Edited by J. W. Schultze) p. 453. Dechema Monographien Band 102, VCH, Frankfurt (1986).
- 42. Yu. V. Pleskov and Yu. Ya. Gurevich, Semiconductor Photoelectrochemistry, p. 297. Consultants Bureau, New York (1986).
- 43. R. W. Haisty, J. electrochem. Soc. 108, 790 (1961).
- 44. H. H. Goossens, F. Vanden Kerchove and W. P. Gomes, J. electroanal. Chem. 261, 89 (1989).
- 45. H. H. Goossens, K. Strubbe and W. P. Gomes, J. electroanal. Chem. **286,** 133 (1990).
- 46. H. H. Goossens, I. E. Vermeir, F. Vanden Kerchove and W. P. Gomes, Electrochim. Acta 35, 1351 (1990).
- 47. R. L. Meek and N. E. Schumaker, J. electrochem. Soc. 119, 1148 (1972).
- 48. M. J. Madou, F. Cardon and W. P. Gomes, Ber. Bunsenges. Phys. Chem. 81, 1186 (1977).
- 49. M. Pourbaix, Atlas d'équilibres électrochimiques, p. 431, p. 510. Gauthier-Villars, Paris (1963).
- 50. D. Vanmaekelbergh and J. J. Kelly, J. electrochem. Soc. 136, 108 (1989).
- 51. D. Vanmaekelbergh, Lu Shou yun, W. P. Gomes and F. Cardon, J. electroanal. Chem. 221, 187 (1987).
- 52. S. Lingier, W. P. Gomes and F. Cardon, Ber. Bunsenges. phys. Chem. 93, 2 (1989).
- 53. P. A. Kohl, C. Wolowodiuk and F. W. Ostermayer Jr, J. electrochem. Soc. 130, 2288 (1983).
- 54. J. J. Kelly, J. E. A. M. van den Meerakker, P. H. L. Notten and R. P. Tijburg, Philips Tech. Rev. 44, 61
- 55. B. Tuck and A. J. Baker, J. mater. Sci. 8, 1559 (1973).
- 56. W. Kern, RCA Rev. 39, 278 (1978).
- 57. A. Yamamoto and S. Yano, J. electrochem. Soc. 122, 260 (1975).
- 58. M. E. Straumanis, J.-P. Krumme and W. J. James, I. electrochem. Soc. 115, 1050 (1968).
- 59. J. van de Ven, A. F. Lourens, J. L. Weyher and L. J. Gilling, Chemtronics 1, 19 (1986).
- 60. A. E. Willner, D. V. Podlesnik, H. H. Gilgen and R. M. Osgood Jr, Appl. Phys. Lett. 53, 1198 (1988).
- 61. J. J. Kelly and A. C. Reynders, Appl. Surf. Sci. 29, 149 (1987).
- 62. H. C. Gatos, Science 137, 311 (1962).
- 63. Y. Mori and N. Watanabe, J. electrochem. Soc. 125, 1510 (1978).

- W.-T. Tsang and S. Wang, Appl. Phys. Lett. 28, 44 (1976).
- 65. S. R. Morrison, Phys. Rev. 104, 619 (1956).
- R. Tenne, V. Marcu and N. Yellin, Appl. Phys. Lett. 45, 1219 (1984).
- 67. R. Tenne and M. Schatkay, Appl. Phys. B 35, 2830 (1984).
- R. Tenne, V. Marcu and Y. Prior, Appl. Phys. A 37, 205 (1985).
- D. E. Aspnes and A. A. Studna, Phys. Rev. B 27, 985 (1983).
- G. Vercruysse, W. Rigole and W. P. Gomes, Solar Energ. Mater. 12, 157 (1985).
- M. M. Faktor and J. L. Stevenson, J. electrochem. Soc. 125, 621 (1978).
- D. E. Williams, A. M. Riley and R. Peat, Proc. SPIE 809, 44 (1987).
- R. Peat, A. Riley, D. E. Williams and L. M. Peter, J. electrochem. Soc. 136, 3352 (1989).
- J.-P. Krumme and M. E. Straumanis, *Trans. AIME* 239, 395 (1967).
- M. J. Madou, F. Cardon and W. P. Gomes, Ber. Bunsenges. phys. Chem. 82, 819 (1978).
- S. Lingier, D. Vanmaekelbergh and W. P. Gomes, J. electroanal. Chem. 228, 77 (1987).
- D. Vanmaekelbergh, J. J. Kelly, S. Lingier and W. P. Gomes, Ber. Bunsenges. phys. Chem. 92, 1068 (1988).
- Lu Shou yun, D. Vanmaekelbergh and W. P. Gomes, Ber. Bunsenges. phys. Chem. 91, 390 (1987).
- A. Etcheberry, J. Gautron, E. M. Khoumri and J. L. Schulfort, J. electroanal. Chem. 283, 177 (1990).
- D. Vanmaekelbergh, W. P. Gomes and F. Cardon: J. electrochem. Soc. 129, 546 (1982).
- K. Strubbe, H. H. Goossens and W. P. Gomes, Electrochim. Acta, in press (1992).
- M. J. Madou, F. Cardon and W. P. Gomes, Ber. Bunsenges. phys. Chem. 82, 819 (1978).
- J. M. Poate, P. J. Silverman and J. Yahalom, J. Phys. Chem. Solids 34, 1847 (1973).
- 84. W. W. Harvey, J. electrochem. Soc. 114, 472 (1967).
- 85. W. J. Plieth, G. Pfuhl, A. Felske and W. Badawy, Electrochim. Acta 34, 1133 (1989).
- 86. P. H. L. Notten, Electrochim. Acta 32, 575 (1987).
- A. Yamamoto, S. Tohno and C. Uemura, J. electrochem. Soc. 128, 1095 (1981).

- C. R. Elliott and J. C. Regnault, J. electrochem. Soc. 128, 113 (1981).
- 89. R. Bhat, J. electrochem. Soc. 132, 2284 (1985).
- P. H. L. Notten, J. E. A. M. van den Meerakker and J. J. Kelly, Etching of III-V Semiconductors: an Electrochemical Approach. Elsevier Advanced Technology, Oxford (1991).
- 91. L. Hollan, J. C. Tranchart and R. Memming, J. electrochem. Soc. 126, 855 (1979).
- F. Decker, B. Pettinger and H. Gerischer, J. electrochem. Soc. 130, 1335 (1983).
- J. J. Kelly and P. H. L. Notten, *Electrochim. Acta* 29, 589 (1984).
- 94. B. P. Minks, G. Oskam, D. Vanmaekelbergh and J. J. Kelly, J. electroanal. Chem. 273, 119 (1989).
- B. P. Minks, D. Vanmaekelbergh and J. J. Kelly, J. electroanal. Chem. 273, 133 (1989).
- B. P. Minks, M. Wiegel and J. J. Kelly, *Electrochim. Acta* 36, 695 (1991).
- J. E. A. M. van den Meerakker, *Electrochim. Acta* 30, 435 (1985).
- P. H. L. Notten, J. electroanal. Chem. 224, 221 (1987).
- P. H. L. Notten and A. A. J. M. Damen, Appl. Surf. Sci. 28, 331 (1987).
- 100. P. H. L. Notten, J. electrochem. Soc. 131, 2641 (1984).
- 101. I. E. Vermeir, to be published.
- I. E. Vermeir, F. Vanden Kerchove and W. P. Gomes, J. electroanal. Chem., 313, 141 (1991).
- J. van de Ven, J. E. A. M. van den Meerakker and J. J. Kelly, J. electrochem. Soc. 132, 3020 (1985).
- 104. J. J. Kelly, J. van de Ven and J. E. A. M. van den Meerakker, J. electrochem. Soc. 132, 3026 (1985).
- 105. J. van de Ven. J. L. Weyher, J. E. A. M. van den Meerakker and J. J. Kelly, J. electrochem. Soc. 133, 799 (1986).
- J. L. Weyher and L. J. Gilling, J. appl. Phys. 58, 219 (1985).
- J. van de Ven and H. J. P. Nabben, J. electrochem. Soc. 137, 1603 (1990).
- J. van de Ven and H. J. P. Nabben, J. electochem. Soc. 138, 144 (1991).
- 109. M. N. Ruberto, X. Zhang, R. Scarmozzino, A. E. Willner, D. V. Podlesnik and R. M. Osgood Jr, J. electrochem. Soc. 138, 1174 (1991).